

Measurements of Ionization Potentials with Laser-induced Plasma Spectroscopy

ASHRAF M. EL SHERBINI¹, MOHAMED M. HAGRASS² AND CHRISTIAN G. PARIGGER^{3*}

¹Laboratory of Laser and New Materials, Faculty of Science, Cairo University, Giza, Egypt

²Faculty of Engineering, Electrical Engineering Department, Alexandria University, Egypt

³The University of Tennessee/University of Tennessee Space Institute, Center for Laser Applications,
411 B.H. Goethert Parkway, Tullahoma, TN 37388-9700, USA

*Corresponding author. E-mail: cparigge@tennessee.edu

ABSTRACT: The first ionization potential of neutral atoms is determined at the thresholds of laser-induced optical breakdown. The induced plasmas at the surface of aluminum, silver, lead, indium and copper are created in laboratory air with focused, 5-ns pulsed Nd:YAG, 1064 nm IR radiation. At fixed spot size of 2 ± 0.1 mm, the laser fluence is varied from 16 to 3 J/cm². For several selected elements that show strong atomic emission lines, the first ionization potentials of Al I 396.2, Ag I 520.9, Pb I 405.8 and 406.2, In I 410.2 and Cu I 515.3 nm are measured to amount to 5.9 ± 0.2 , 7.6 ± 0.3 , 7.4 ± 0.2 , 5.8 ± 0.1 and 7.7 ± 0.2 eV, respectively. The measured ionization energies for the different targets nicely agree with tabulated values, consequently, this agreement can be interpreted as confirmation for the laser-induced plasma threshold model.

PACS Codes: 52.38.Mf, 52.70.-m, 32.30.-r, 52.25.Jm, 42.62.Fi, 82.80.-d

Keywords: Laser ablation, plasma diagnostics, atomic spectroscopy, plasma ionization, laser spectroscopy.

1. INTRODUCTION

The generation of laser-induced plasma requires sufficient irradiance to initiate the avalanche type optical breakdown process [1-9]. Plasma is described as the fourth state of matter and is mainly composed of four different species: Atoms, electrons, ions and radiation field that are distributed according to well-known equilibrium distribution functions. The minimum energy flux required for plasma formation is called threshold fluence, ϕ_{th} (J/cm²). The fluence thresholds [1-9] depend on thermal parameters of the material that include density, latent heat of vaporization, coefficient of thermal conductivity and specific heat as well as on laser excitation wavelength and ionization energy [1, 2, 10-12].

In this work, bulk metallic targets are investigated to infer the ionization potentials [13] using selected lines of aluminum, silver, lead, indium and copper. The measured first ionization potentials are expected to agree with published values, thereby confirming the model for the breakdown thresholds of bulk material [1, 2].

2. LASER-INDUCED THRESHOLD

At the laser irradiance threshold, the amount of laser energy just needed to vaporize the target material in the laser focal volume is given by the thermal term [5], $\phi_{th}^{thermal}$, which is constant for each material and can be calculated from classical material-dependent properties. However, in order to ionize this vapor, an additional laser-dependent term [1, 2],

$$\phi_{th}^{laser} = C \frac{\epsilon_i}{\lambda_{laser}^2} l_T, \quad (11)$$

needs to be considered [1, 2]. Here, l_T is the thermal conduction or diffusion length (m), λ_{laser} is the laser wavelength and ϵ_i is the first ionization potential energy. The threshold term for the laser fluence, ϕ_{th}^{laser} , originates from the time-averaged ponderomotive energy for linear polarization [14, 15]. The proportional relation of the threshold laser fluence with the inverse square laser wavelength and linear thermal conduction length was already studied for nano-materials of different sizes [2, 3, 4]. The constant C is composed of a combination of electromagnetic constants [1], including m_e , ϵ_0 , c and e denoting mass of the electron, vacuum permittivity, speed of light and elementary charge, respectively,

$$C = 8\pi^2 m_e \epsilon_0 c^2 / e^2 = 2.235 \times 10^{15} (m^{-1}). \quad (2)$$

Recent work discussed measurements of thresholds, ϕ_{th} , and confirmed that the complimentary laser-dependent contribution, ϕ_{th}^{laser} , at different laser irradiation wavelengths needs to be added to describe fluence thresholds of laser-induced plasma at the surface of bulk material [1, 2],

$$\phi_{th} = \phi_{th}^{thermal} + 2.235 \times 10^{15} \frac{\epsilon_i}{\lambda_{laser}^2} l_T. \quad (3)$$

The thermal contribution, $\phi_{th}^{thermal}$, amounts to

$$\phi_{th}^{thermal} = \rho L_v l_T, \quad (4)$$

and the thermal conduction or diffusion length [1, 2, 5], l_T , can be expressed as

$$l_T = \sqrt{\kappa_T \tau_{laser} / \rho C_p}, \quad (5)$$

where κ_T is the thermal conductivity coefficient of the material (W/m K), ρ is the density (kg/m³), τ_{laser} is the laser pulse duration (s), C_p is the specific heat at constant pressure (J/kg K) and is the latent heat of vaporization in (J/kg).

For the evaluation of the ionization energies, Eq. (3) is suggested and applied in this work, and it can be expressed in frequently encountered units for laser fluence, wavelength and thermal conduction length,

$$\epsilon_i (eV) = 27.9 \left[\phi_{th} - \phi_{th}^{thermal} \right] (J/cm^2) \frac{\lambda_{laser}^2}{l_T} (\mu m). \quad (6)$$

In this formula, ϕ_{th} should be larger than the classical thermal vaporization term, $\phi_{th}^{thermal}$. Therefore, at a fixed laser irradiation wavelength and with knowledge of classical properties, one can measure the ionization potential, ϵ_i , by decreasing the laser energy to find the fluence threshold, ϕ_{th} , for plasma generation.

3. EXPERIMENTAL DETAILS

The experimental configuration for the ionization energy measurements includes a Q -switched Nd:YAG laser device, focusing and attenuation optics, and optical fiber coupled to a spectrometer equipped with an intensified detector [1, 2]. The Nd:YAG pulsed laser is operated at the fundamental wavelength, $\lambda_{laser} = 1064$ nm, with pulse duration, $\tau_{laser} = 5$ ns, delivering an output energy of 470 mJ per pulse. The laser radiation is focused with a convex lens of 1 m focal length. The focal spots show radii of 2 ± 0.1 mm, measured using thermal heat sensitive paper (Kentek or Quantel® heat sensitive paper).

The laser fluences are varied in the range of 16 to 3 J/cm² with a set of calibrated glass attenuators. The variation of the laser radiation is monitored using a 4% reflective beam splitter with an absolutely calibrated power

meter (Ophir model 1z02165). The emitted radiation from the plasma is collected with an optical fiber of 25 μm diameter, connected to the detection system comprised of a spectrograph (SE 200 Echelle Spectrograph) and an intensified charge coupled device (ICCD Andor-iStar DH734-18F). The camera is used to record the time-resolved spectra in the range of 200 to 1000 nm. The fiber tip is positioned at a distance of 18 ± 2 mm from the plasma expansion axis. Absolute calibration of the detector system is accomplished with a deuterium-halogen light source (Ocean Optics® DH-2000-CAL) [16].

In order to obtain clear optical signals from different plasmas, the light emissions were collected over three different laser shots. The strongest spectral line intensity for each material was selected, *e.g.*, the In I at 410.17 nm and Al I at 396.15 nm lines. The isolated lines are selected to record the plasma emission at different irradiation levels, and the signal to background ratio, S/B, is monitored.

4. RESULTS AND DISCUSSION

The target materials used in our work are selected to cover a relatively wide range of expected threshold values from 0.4 for Pb to 3.5 J/cm² for Cu and diverse thermal properties.

Table 1 summarizes the thermal and physical parameters. This table shows that there is an apparent increase of isobaric specific heat of materials except for aluminum which has relatively large heat capacity. There is an apparent increase in the thermal conductivity (κ_T) and latent heat of vaporization (L_v) except for copper and aluminum. Neither one of the physical quantities is responsible of the threshold of plasma ignition alone but only a combination of these quantities may be responsible for the generation of laser-induced plasma.

Table 1

Thermal and physical parameters of the elements used in this work in SI units for density, ρ , latent heat of vaporization, L_v , thermal conductivity coefficient, κ_T , specific heat (isobaric), C_p (J/kg K) and recommended wavelength, λ (nm). For indium and aluminum, lines emerging from resonance transitions are indicated. The listed data are taken from the NIST data base [17].

	r (kg/m ³)	L_v (10 ⁶ J/kg)	κ_T (W/m K)	C_p (J/kg K)	λ (nm)
Pb	11350	1.8	35	130	406.00
In	7300	1.9	83.7	233	410.17
Al	2700	10.8	237	900	396.15
Ag	10500	2.4	429	237	520.90
Cu	8960	4.8	401	385	515.32

Regarding the lead Pb I line, the midpoint 406.00 nm of the two prominent lines at wavelengths of 405.78 and 406.21 nm is considered because they appear actually as a single line even at lower laser irradiance levels. Stark broadening and choice of resolution instrumental bandwidth (0.12 nm) resulted in overlap of the two lines separated by 0.5 nm.

Table 2 shows the variation of the combination of thermal conductivity, specific heat, density and laser pulse duration, labeled thermal conduction length, l_T , and the heat enthalpy per unit volume, ρL_v (J/m³). The table also shows the thermal term, $\phi_{th}^{thermal}$, see Equation (4). The investigated elements are arranged in Table 1 in ascending order of the predicted threshold laser fluences according to Eq. (6) at the laser wavelength of 1064 nm.

As can be noted from the data in Table 2, there is an increase from Pb to Cu in the thermal conduction length and the density \times heat enthalpy product of the materials except for silver because of its relatively large thermal conductivity. The thermal contribution, $\phi_{th}^{thermal} = \rho L_v l_T$, shows an increase but is consistently smaller than the theoretically predicted contribution from the laser fluence, ϕ_{th}^{laser} , indicated in Eq. (3).

Figure 1 illustrates typical recorded copper emission spectra. The integrated spectral intensity is obtained by evaluating the area of the lines after subtracting the continuum or background.

Table 2
Element parameters: Density \times heat enthalpy product, ρL_v , thermal conduction length, l_T , thermal term, $\phi_{th}^{thermal}$, and predicted thresholds from Equation (6), ϕ_{th} .

	ρL_v (kJ/cm ³)	l_T (nm)	$\phi_{th}^{thermal}$ (J/cm ²)	ϕ_{th} (J/cm ²)
Pb	9.7	350	0.33	0.42
In	14	500	0.70	0.80
Al	28	700	1.97	2.10
Ag	25	1000	2.3	2.55
Cu	43	760	3.27	3.46

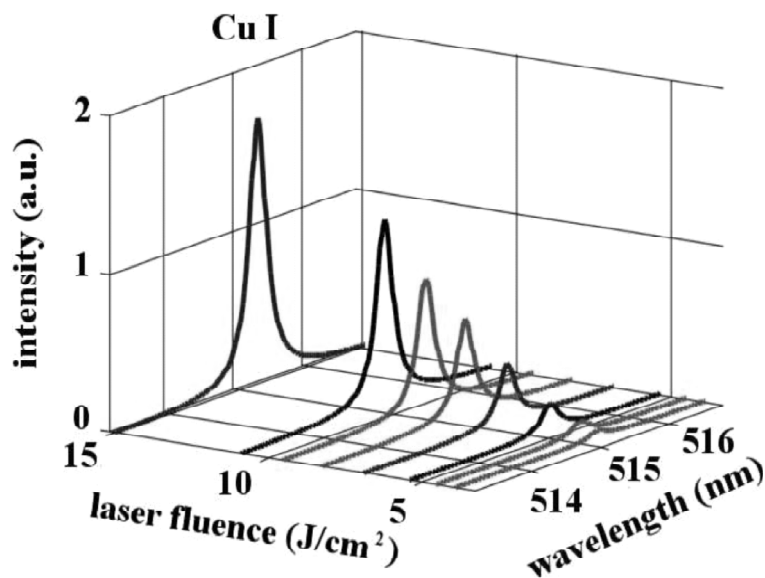


Figure 1: Measured spectra of the 515.32 nm Cu I line versus wavelength and laser fluence.

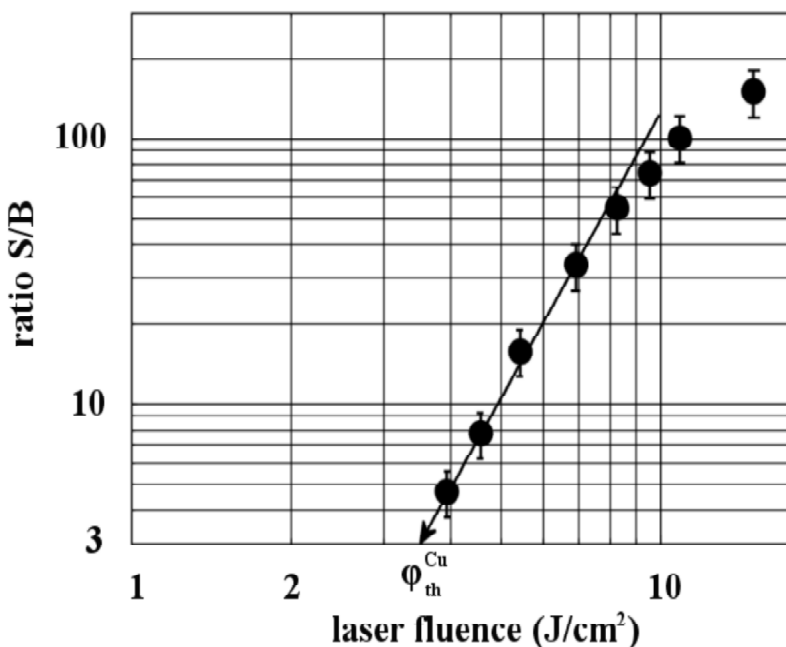


Figure 2: Signal to background ratio, S/B, for the 515.32 nm Cu I line and threshold, $\phi_{th}^{Cu} = 3.4$ J/cm², at S/B = 3.

The plasma-threshold fluence is determined *via* backward extrapolation at the recommended signal-to-background, S/B, value of three as indicated in Figure 2. The log-log plot in Figure 2 shows a linear decrease in the S/B ratio for smaller laser fluences in the range of 10 to 3 J/cm². For larger signal levels, the recorded spectral intensities of the lines tend to saturate. The saturation may be attributed to self-absorption effects at the relatively large laser fluences.

Table 3
Measured thresholds, ϕ_{th}^{exp} , ionization energies, ϵ_i , and comparison with tabulated ionization energies, ϵ_{tab} , and work functions, W_{tab} , for bulk metallic targets.

	ϕ_{th}^{exp} (J/cm ²)	ϵ_i (eV)	ϵ_{tab} (eV)	W_{tab} (eV)
Pb	0.42 ± 0.04	7.4 ± 0.2	7.4	4.1
In	0.80 ± 0.05	5.8 ± 0.1	5.8	4.1
Al	2.10 ± 0.07	5.9 ± 0.2	5.9	4.1
Ag	2.55 ± 0.10	7.6 ± 0.3	7.6	4.7
Cu	3.40 ± 0.07	7.7 ± 0.2	7.7	4.7

Table 3 shows the experimentally measured laser threshold fluences corresponding to each element, the measured first ionization energy utilizing the plasma threshold laser fluence, the tabulated standard values for the ionization energies and for the work functions. The work function is defined as the minimum energy required generating free electrons from the surface of a solid. The work functions of the different elements show nearly constant values in the range of 4.1 to 4.7 eV. However, the discussed model for laser-induced breakdown thresholds in laboratory air at standard ambient temperature and pressure, indicates that the ionization energy is the significant term for fluence thresholds in Eq. (6) rather than work function.

Excellent agreement of measured and tabulated first ionization potentials can be noticed in Table 3 for the different elements. This agreement can be viewed as a further confirmation of the validity of the laser term as suggested previously in generation of plasma in laboratory air at or near the surface of different target materials [1, 2].

5. CONCLUSION

The laser induced plasma threshold dependence on laser wavelength and ionization energy was utilized to provide means to measure the first ionization potential of elements. The measured ionization energies for the different targets nicely agree with tabulated values. In turn, this agreement can be interpreted as confirmation for the laser-induced plasma threshold model. As an extension to this work, studies with different laser wavelengths will be reported.

ACKNOWLEDGMENT

The authors acknowledge the continued interest and comments from Professor Th. M. EL Sherbini and thank for support in part by the Center for Laser Applications at the University of Tennessee Space Institute and in part by the Laboratory of Laser and New Materials at Cairo University.

REFERENCES

- [1] A.M. EL Sherbini, C.G. Parigger, Spectrochim. Acta Part B **116** (2016) 8.
- [2] A.M. EL Sherbini, C.G. Parigger, Spectrochim. Acta Part B **124** (2016) 79.
- [3] E.G. Gamaly, A.V. Rode, B. Luther-Davies, J. Appl. Phys. **85** (1999) 4213.

- [4] A.V. Rode, B. Luther-Davies, E.G. Gamaly, *J. Appl. Phys.* **85** (1999) 4222.
- [5] L.M. Cabalin, J.J. Laserna, *Spectrochim. Acta Part B* **53** (1998) 723.
- [6] B.W. Boreham, J.L. Hughes, *Sov. Phys. JETP* **53** (1981) 252.
- [7] D.X. Hammer, R.J. Thomas, G.D. Noojin, B.A. Rockwell, P.K. Kennedy, W.P. Roach, *IEEE J. Quantum Electron.* **32** (1996) 670.
- [8] T.X. Phuoc, *Opt. Commun.* **175** (2000) 419.
- [9] S. Brieschenk, H. Kleine, S. O'Byrne, *J. Appl. Phys.* **114** (2013) 093101.
- [10] A.E. Hussein, P.K. Diwakar, S.S. Harilal, A. Hassanein, *J. Appl. Phys.* **113** (2013) 143305.
- [11] A. Vogel, K. Nahen, D. Theisen, J. Noack, *IEEE J. Sel. Top. Quantum Electron.* **2** (1996) 847.
- [12] N. Linz, S. Freidank, X. Liang, H. Vogelmann, T. Trickl, A. Vogel, *Phys. Rev. B* **91** (2015) 134114.
- [13] S. Rothe, A.N. Andreyev, S. Antalic, A. Borschevsky, L. Capponi, T.E. Cocolios, H. De Witte, E. Eliav, D.V. Fedorov, V.N. Fedosseev, D.A. Fink, S. Fritzsche, L. Ghys, M. Huyse, N. Imai, U. Kaldor, Yuri Kudryavtsev, U. Köster, J.F.W. Lane, J. Lassen, V. Liberati, K.M. Lynch, B.A. Marsh, K. Nishio, D. Pauwels, V. Pershina, L. Popescu, T.J. Procter, D. Radulov, S. Raeder, M.M. Rajabali, E. Rapisarda, R.E. Rossel, K. Sandhu, M.D. Seliverstov, A.M. Sjödin, P. Van den Bergh, P. Van Duppen, M. Venhart, Y. Wakabayashi, K.D.A. Wendt, *Nat. Commun.* **4** (2013) 1835.
- [14] P. Mulser, D. Bauer, *High Power Laser-Matter Interaction*, Springer Verlag, Heidelberg, DE, 2010.
- [15] W. Lotz, *J. Opt. Soc. Am.* **57**(1967) 873.
- [16] A.M. EL Sherbini, A.M. Aboufotouh, C.G. Parigger, *Spectrochim. Acta Part B* **125** (2016) 152.
- [17] A. Kramida, Yu. Ralchenko, J. Reader, and NIST ASD Team (2016). NIST Atomic Spectra Database (version 5.4), [Online]. Available: <http://physics.nist.gov/asd> [Fri Dec 09 2016]. National Institute of Standards and Technology, Gaithersburg, MD; <https://www.nist.gov/pml/atomic-spectra-database> (last accessed 9/24/2016).